doi:10.26443/seismica.v5i1.1893

Seismic Swarms Occurrence Rate and b-value Mapping at Taupō Volcanic Zone

Giuseppe Petrillo [1], **Vincenzo Convertito** [2], **Anna Tramelli** [*2], **Cataldo Godano** [3]

[1]CNRS, ENS de Lyon, LPENSL, UMR5672, 69342, Lyon cedex 07, France, [2]Istituto Nazionale di Geofisica e Vulcanologia, Sezione di Napoli - Osservatorio Vesuviano, Via Diocleziano, 328, 80124 Napoli, Italy, [3]Università della Campania "L. Vanvitelli" Dipartimento di Matematica e Fisica Viale Lincoln 5 - 81100 Caserta - Italy

Author contributions: *Conceptualization*: Giuseppe Petrillo, Vincenzo Convertito, Anna Tramelli, Cataldo Godano. *Formal Analysis*: Giuseppe Petrillo, Vincenzo Convertito, Anna Tramelli, Cataldo Godano. *Writing - Original draft*: Giuseppe Petrillo, Vincenzo Convertito, Anna Tramelli, Cataldo Godano.

Abstract We analyze the seismicity of the Taupō Volcanic Zone (TVZ) over a 17-year period (2007-2024) using a swarm-informed ETAS model and high-resolution b-value mapping. To better describe swarm dynamics, marked by rapid, clustered activity without a mainshock, we introduce a modified Epidemic Type Aftershock Sequence (ETAS) kernel with finite memory and exponential tapering, which explicitly accounts for the finite duration of seismic swarm activity. This new model outperforms the classical ETAS, capturing the full temporal evolution of swarm sequences. The inferred rate highlights recurrent swarm episodes and captures known unrest periods in the TVZ (e.g., the 2019 Taupō unrest), illustrating how the proposed kernel can represent multi-swarm, non-Omori temporal clustering. Moreover, using the unstruCtUred B mappIng Tool CUBIT algorithm and the b-more-positive estimator, we map spatial and temporal variations in the b-value. Higher b-values are observed in younger, hotter volcanic centers, while older systems show lower values. A subtle positive skewness in the b-value distribution is linked to local magnitude range effects, underscoring the interplay between catalog completeness and stress heterogeneity. Our results highlight the importance of combining physically informed models with robust statistical tools to understand and monitor volcanic swarm activity.

Production Editor:
Yen Joe Tan
Handling Editor:
Lise Retailleau
Copy & Layout Editor:
Mengjie Zheng

Signed reviewer(s):
M. Laporte
M.-S. Seo

Received:
July 25, 2025
Accepted:
April 19, 2026
Published:
May 28, 2026

1 Introduction

Statistical properties of earthquake occurrence can be described in terms of spatial and temporal clustering, as well as by the distribution of magnitudes.

Time clustering properties are, generally, defined by the Omori-Utsu law (Omori, 1894):

$$n = \frac{k}{(t+c)^p} \tag{1}$$

where n is the number of earthquakes, t is the time elapsed from the occurrence of the mainshock, c is a delay time during which n assumes a constant value, p controls the n decay speediness and k is a normalization factor depending on the mainshock magnitude (Helmstetter, 2003). The Omori law is a milestone of statistical seismology for the temporal characterization of earthquake occurrence as testified by the huge amount of literature produced on the argument (see among the others Utsu et al. (1995) and references therein). It represents a crucial ingredient of the Epidemic Type Aftershock Sequences (ETAS) model (Ogata, 1985, 1988, 1998) and of its development (Kumazawa and Ogata, 2014; Xiong and Zhuang, 2023; Liu et al., 2024; Petrillo and Zhuang, 2024; Petrillo et al., 2024b,a; Petrillo and Taroni, 2025). However, it is not able to capture the behavior of seismic swarms, which generally occur in volcanic areas.

Swarms are groups of earthquakes clustered in time and space without any mainshock (Knett, 1899) and their occurrence has been associated with pore pressure changes (Miller et al., 2004), fluid intrusion (Toda et al., 2002; Gentili et al., 2024), tectonic stress changes (Mesimeri et al., 2018) and medium heterogeneity (Mogi, 1962). More recently Godano et al. (2023) introduced a new expression for swarms occurrence rate described in terms of a Gamma distribution. In what follows we introduce such expression as a kernel of an epidemic model and compare it with a standard ETAS model showing that the Gamma distribution model better describes the behavior of the catalogue here analyzed.

The ability to model and interpret earthquake swarms thus relies on two complementary dimensions: the temporal clustering of the events, and the distribution of their magnitude. While the former can be addressed through point-process models such as ETAS and its swarm-informed extensions, the latter is encapsulated in the Gutenberg-Richter (GR) (Gutenberg and Richter, 1944) law through the b-value. Both aspects are critical to understand the physical processes driving swarm activity and to identify possible precursory signals. In the next section, we shift our focus from rate-based modeling to a detailed statistical analysis

*Corresponding author: anna.tramelli@ingv.it

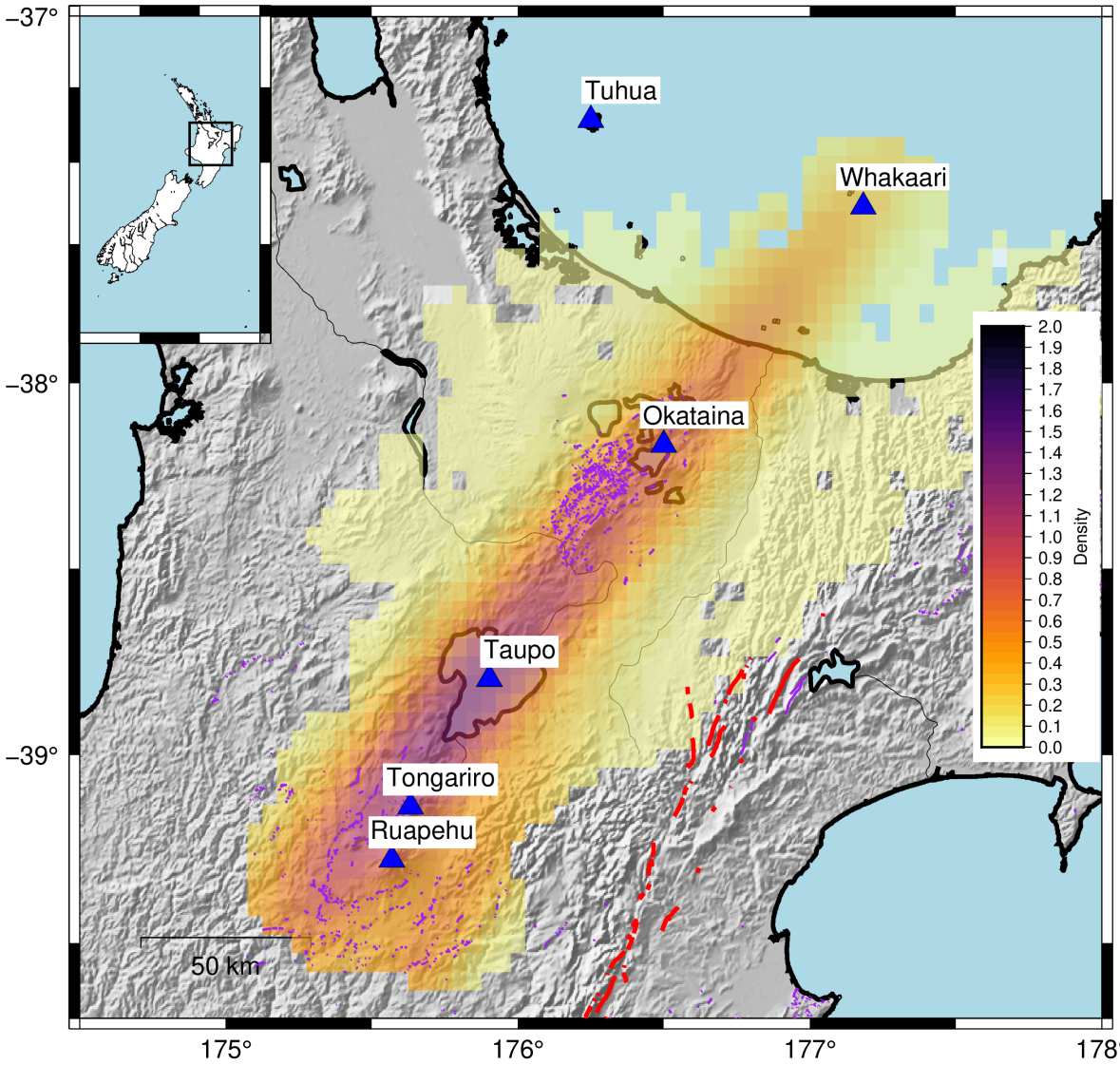

Figure 1 Geographic map of the Kernel density of the epicenter of the earthquakes analyzed in this study. Blue triangles identify the volcanoes. Active fault traces are from the New Zealand Active Faults Database (GNS Science; Morgenstern et al., 2024). All mapped faults are shown (purple lines) for comprehensive seismotectonic context, with higher-slip-rate faults highlighted in red.

of the magnitude distribution, placing particular emphasis on the robustness and spatial variability of the b-value in the Taupō Volcanic Zone (TVZ), New Zealand.

The GR law states that the cumulative number of earthquakes with magnitude $\geq m$ follows an exponential law:

$$\log_{10} N(m) = a - bm, \tag{2}$$

where a is a normalization constant and b is the scaling exponent. In practice, the estimation of b requires selecting a minimum magnitude m_c above which the catalog is complete.

The completeness magnitude m_c strongly influences the estimate of the value b. In particular, if m_c is underestimated, the value of b is also underestimated. In contrast, when m_c is overestimated, the magnitude range can be small, causing an increase in the estimation error. Recently, van der Elst (2021b) suggested to use the distribution of δm (the positive difference of magnitude between two successive earthquakes). δm follows the Laplace distribution and allows a very efficient b-value estimate being independent of m_c. The method has been named b-positive and it has been extended to the b-more-positive method by Lippiello and Petrillo (2024).

The importance of the b-values relies on its proportionality with differential stress (Scholz, 1968; Wyss, 1973; Amitrano, 2003; Gulia and Wiemer, 2010) and with the heterogeneity of the medium (Mogi, 1962). As a consequence, the investigation of this parameter has produced a large amount of literature (see, among others, Wiemer and Wyss, 1997, 2002; Westerhaus et al., 2002; D. et al., 2005; Tormann et al., 2014; Kamer and Hiemer, 2015; Gulia et al., 2018; Taroni et al., 2021; Collettini et al., 2022; Godano et al., 2022a; Pino et al., 2022; Godano et al., 2022b; Convertito et al., 2024a,b; Taroni et al., 2025).In volcanic and geothermal regions, spatial variations of the b-value have been repeatedly linked to the thermo-mechanical state of the crust, with higher b-values often reported in hotter, more fractured and fluid-rich volumes (e.g., Wiemer and McNutt, 1997; Wiemer et al., 1998; Jolly and McNutt, 1999; Murru

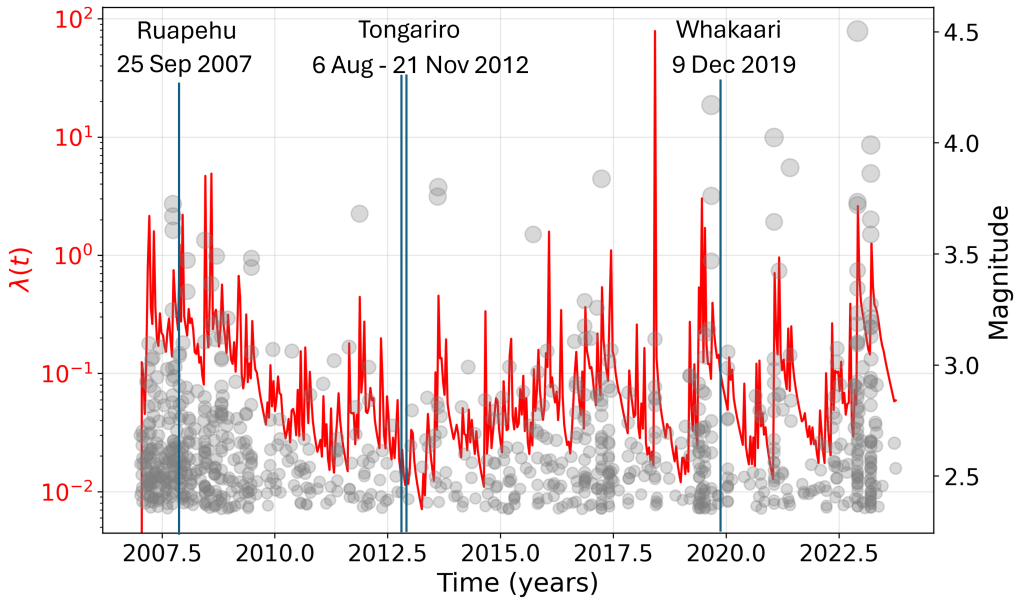

Figure 2 Temporal evolution of the seismic occurrence rate $\lambda(t)$ inferred from the swarm-informed ETAS model (red curve), together with the observed seismicity in the Taupō Volcanic Zone. Each gray circle represents an earthquake, with marker size proportional to magnitude. Time is expressed in decimal years, providing a direct reference to calendar time and facilitating comparison with periods of volcanic unrest. The figure highlights the strongly nonstationary character of the seismicity, with repeated short-lived rate transients typical of swarm-like activity.

et al., 1999; Sanchez et al., 2004; Bridges and Gao, 2006; Murru et al., 2007; Farrell et al., 2009; Silva et al., 2015; Chiba and Shimizu, 2018; Rodríguez-Pérez et al., 2021; Tramelli et al., 2021; Godano et al., 2024b; Convertito et al., 2025). More broadly, recent studies have emphasized the sensitivity of b-value patterns to magma migration and fluid pressurization during volcanic unrest, motivating the use of magnitude statistics as a quantitative monitoring tool. For instance, studies in the Santorini volcanic complex reported systematic spatial variations of b, highlighting the sensitivity of magnitude statistics to volcano-tectonic processes (Lippiello et al., 2025b; Zaccagnino et al., 2025; Triantafyllou et al., 2025; Oynakov et al., 2025).

Time variations of b have been also observed and proposed as a tool in earthquake forecasting (Gulia and Wiemer, 2019; Gulia et al., 2020; Godano et al., 2024c, 2025b). In fact, changes in b-value before or after a large earthquake indicate the occurrence of foreshocks (Papale, 2018; Papadopoulos et al., 2010) or help distinguish between foreshocks and mainshocks (Gulia and Wiemer, 2019; Petrillo and Lippiello, 2021, 2023; Lippiello et al., 2025a).

Maps of the b-value have been produced to delineate its spatial variation and to correlate them with the stress state of the crust (Scholz, 1968; Amitrano, 2003; Tormann et al., 2014). The maps are usually evaluated by gridding the space to group the earthquakes and by assuming a single b-value for each grid unit. In some cases, the earthquakes are grouped on the basis of the fault style (e.g., Gulia and Wiemer, 2010). More often, maps are produced by gridding the space into constant-size cells (e.g., Wiemer and Wyss, 1997, 2002). Then earthquakes are selected according to some rules (minimum number of events, maximum distance from the center of the cell, etc.). In what follows, we investigate the seismicity of the Taupō Volcanic Zone using a combination of complementary statistical analyses. We first analyze the temporal evolution of seismicity through a swarm-informed ETAS model, aimed at capturing the characteristic rate variations associated with volcanic swarms. We then investigate the spatial distribution of the Gutenberg-Richter b-value using the unstruCtUred B mappIng Tool (CUBIT) highlighting correlations between b-values and the age of the volcanic centers. Finally, we explore the temporal variations of the b-value to assess transient stress changes accompanying swarm activity.

2 Taupō Volcanic Zone and the seismic catalogue

The TVZ is a $\sim$ 300 km long extensional region in the North Island of Aotearoa, New Zealand, known for its intense volcanic and seismic activity. It hosts multiple active volcanic centers such as Taupō, Okataina, Tongariro, and Ruapehu, and it is characterized by a high heat flow and extensive geothermal systems. The TVZ is the on-land part of the Tonga-Kermadec back-arc rift system, capable of producing both swarm-type seismicity and larger tectonic earthquakes (e.g., the 1987 Mw=6.5 Edgecumbe earthquake). Although tectonic earthquakes do occur in the TVZ, their contribution to the 2007-2024 seismic catalog analyzed here is limited compared to the pervasive swarm-like seismicity associated with volcanic and geothermal processes, which dominates the temporal clustering properties of the dataset. Seismicity in this region often reflects the interplay between magmatic processes, hydrothermal activity, and rift dynamics.

It is the on-land part of the Tonga-Kermadec rifting arc, caused by the Australian and Pacific plates converging. The Taupō Volcanic Zone hosts volcanic centers with a wide range of constructional ages, including Ruapehu ($\sim$ 340 ka; Leonard et al., 2021), Tongariro ($\sim$ 300 ka; Pure et al., 2020), Taupō ($\sim$ 255 ka; Barker et al., 2021), Whakaari ($\sim$ 150 ka; Cole et al., 2000), and Ōkataina ($\sim$ 500 ka; Shane and Smith, 2013). These ages reflect the long-lived evolution of the volcanic arc and do not necessarily correspond to present-day magmatic or seismic activity. For our analysis, we use the high-precision earthquake catalogue developed by Illsley-Kemp and Mestel (2025), covering the period from January 2007 to December 2023. Figure 1 depicts the kernel density, which provides the probability density function of the earthquakes' epicentral distribution. This catalogue includes 86,579 earthquakes located within the crustal portion of the TVZ (depths shallower than 50 km), and represents a significant improvement in spatial resolution compared to previous national catalogues. Approximately 65% of these events have been relocated using differential travel time methods and a 3D seismic velocity model tailored to the North Island, providing high-resolution hypocentral information.

The magnitude range spans from $M_L = -1.2$ to $M_L = 4.5$, with a completeness magnitude of $m_c = 2.35$ estimated using the method introduced by Godano et al. (2024a). A magnitude cutoff is required only for the ETAS-based temporal analysis, which assumes an approximately stationary detection capability. In contrast, both the spatial and temporal b-value analyses are performed using the b-more-positive method, which does not require an explicit estimate of the magnitude of completeness and can therefore exploit the full catalog.

The catalogue reveals a highly heterogeneous spatiotemporal distribution of seismicity. Shallow events dominate beneath Ruapehu and Tongariro, while mid-crustal activity (8-20 km depth) is prevalent beneath Taupō and Okataina. Persistent seismic swarms are also observed in specific geothermal fields (e.g., Waihi–Hipaua), suggesting fluid-driven processes. The high resolution and consistency of this catalogue make it ideally suited for investigating both the temporal clustering of events through point-process modeling and the spatial variability of the Gutenberg–Richter b-value.

3 Swarm-informed temporal kernel and ETAS modeling

A key challenge in statistical seismology is to correctly model the rate at which earthquakes occur during swarm episodes, especially in volcanic environments. Unlike classical mainshock-aftershock sequences, swarms typically consist of many events clustered in time and space but lacking a clearly identifiable mainshock. This behavior is often driven by non-tectonic mechanisms such as magma intrusions, fluid pressurization, or hydrothermal activity, and cannot be fully captured by standard models based on stress redistribution from a single large rupture.

In what follows, we do not attempt to identify individual swarm episodes a priori. Instead, we model the conditional seismicity rate of the entire catalog using a triggering kernel whose temporal form is motivated by the phenomenology of volcanic swarms. In this sense, the proposed formulation should be interpreted as a swarm-informed ETAS model, rather than a method that explicitly isolates a pure swarm-only occurrence rate. The Epidemic-Type Aftershock Sequence (ETAS) model (Ogata, 1989, 1998) is one of the most widely used frameworks to describe clustered seismicity. In its classical formulation, the ETAS model assumes that each earthquake can trigger subsequent events, with the total conditional intensity $\lambda(t)$ at time t given by:

$$\lambda(t) = \mu + \sum_{t_i<t} K\, e^{\alpha(m_i - M_0)} \frac{1}{Z(p,c)} (t - t_i + c)^{-p}, \quad (3)$$

$$\texttt{with} \quad Z(p,c) = \frac{c^{1-p}}{p-1}$$

where μ is the background rate of spontaneous (Poissonian) events, K represents the average number of aftershocks triggered by an event of magnitude m_i, and p and c control the shape and onset of the normalized temporal decay kernel, respectively. The term $Z(p,c)$ ensures that the triggering kernel integrates to one. Despite its success in modeling tectonic sequences, the classical ETAS model has several limitations in volcanic settings:

- It assumes a long-tailed power-law memory kernel that decays too slowly to reproduce the rapid onset and termination of swarm activity.
- It does not account for physical processes such as fluid injection or viscoelastic relaxation that can truncate the triggering process at finite times.
- The assumption of a triggering process driven entirely by earthquake-induced stress transfer may not hold when aseismic forces dominate.

To address these issues, Godano et al. (2023) proposed an alternative expression for the average occurrence rate of earthquakes during volcanic swarms. By first identifying swarm episodes based on space-time clustering criteria and then stacking the selected sequences, they showed that the average occurrence rate of volcanic swarms can be well described by the function:

$$\nu(t) \propto \left(t^{-p} + \mu\right) e^{-t/\tau}, \quad (4)$$

where p controls the initial power-law decay, μ introduces a plateau or bump at intermediate times, and the exponential taper $e^{-t/\tau}$ captures the finite duration of swarm activity. This form naturally ensures that the occurrence rate is normalizable even when $c = 0$, and was interpreted in terms of impulsive stress perturbations and viscoelastic relaxation of the crust. In that study, swarm sequences were explicitly identified prior to the analysis, and the function above represents an average swarm rate obtained from stacked sequences. In the present work, we do not perform such a prior classification. Instead, we use this empirically derived functional

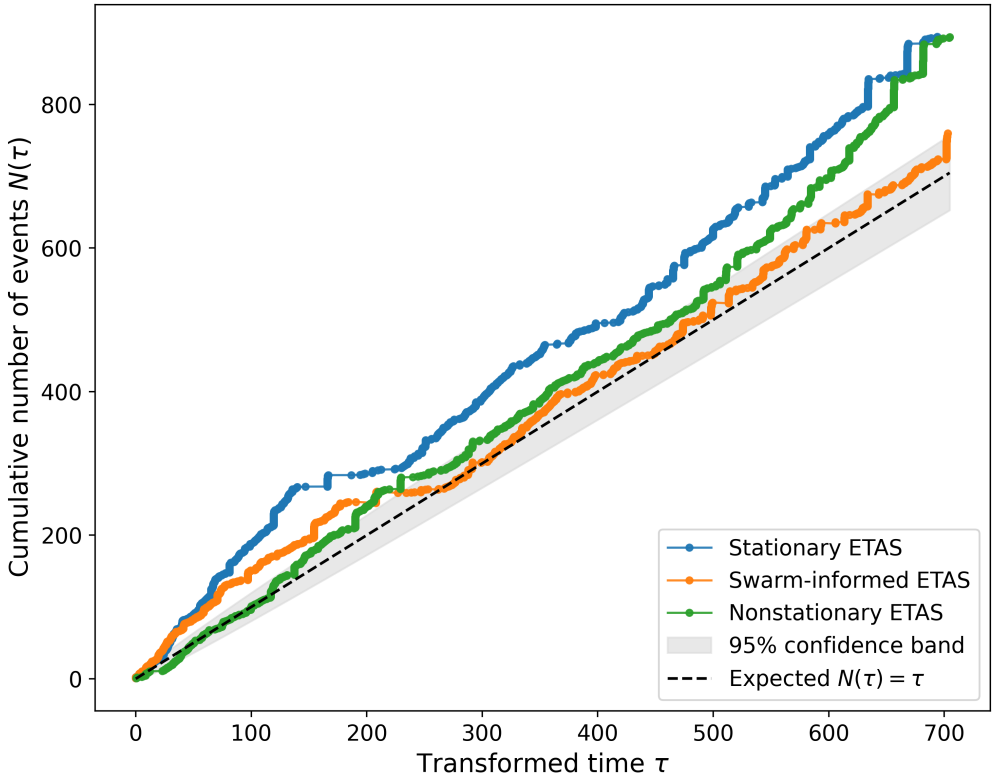

Figure 3 Cumulative number of events $N(\tau)$ as a function of the transformed time $\tau = \int_{T_1}^{t} \lambda(u \mid \mathcal{H}_u)\, du$ for the three temporal models considered: stationary ETAS (blue), swarm-informed ETAS (orange), and nonstationary ETAS (green). Under a correctly specified conditional intensity, the rescaled process is a unit-rate Poisson process and the expected behavior is $N(\tau) = \tau$ (black dashed line). The shaded area indicates the 95% confidence band for a Poisson process with unit rate. Deviations from the diagonal quantify systematic misfit of the temporal model, independent of parameter dimensionality. The swarm-informed ETAS model closely follows the expected behavior and performs comparably to the nonstationary ETAS, while the stationary ETAS shows larger departures, particularly at intermediate and late transformed times.

form as a temporal kernel within an ETAS framework to model the overall seismicity.

Inspired by this functional form, we introduce a modified ETAS model in which the classical Omori-type kernel is replaced by a swarm-informed kernel. The resulting conditional intensity is given by:

$$\lambda(t) = \sum_{t_i<t} K e^{\alpha(m_i - M_0)} \frac{e^{-(t-t_i)/\tau}\,[\mu + (t-t_i)^{-p}]}{Z(\tau, p, \mu)}, \quad (5)$$

where the summation runs over all previous events $\{t_i\}$ and the kernel is explicitly normalized via the factor

$$Z(\tau, p, \mu) = \mu\tau + \tau^{1-p}\Gamma(1-p). \quad (6)$$

This normalization ensures that the integral of the kernel over the interval $t \in [0, \infty)$ is equal to one:

$$\begin{aligned} \int_0^\infty \left[\mu + t^{-p}\right] e^{-t/\tau}\, dt &= \mu\,\tau + \tau^{\,1-p}\,\Gamma(1-p) \\ &= Z(\tau, p, \mu), \end{aligned} \quad (7)$$

allowing the kernel to be interpreted as a proper probability density and enabling the computation of the conditional log-likelihood without further numerical approximations.

It is important to note that Eq. (5) defines the conditional intensity of the full seismicity process, and therefore includes contributions from all triggering interactions in the catalog. The term "swarm-informed" refers to the choice of the temporal kernel, which is designed to reproduce the typical temporal evolution of swarm-like sequences, rather than to an explicit separation between swarm and non-swarm events. Compared to classical ETAS, this formulation introduces a *finite memory timescale* τ, while preserving the short-time clustering behavior governed by p. The exponent p controls the early-time decay of the triggering process, similarly to the Omori law, but the exponential taper $e^{-t/\tau}$ imposes a finite duration of the triggering memory, preventing the unrealistically long-tailed behavior typical of classical ETAS kernels. The parameter τ can therefore be interpreted as a characteristic timescale over which the triggering efficiency remains significant, and is consistent with the finite duration of swarm activity observed in volcanic environments. The additive μ term, which is part of the triggering kernel itself, introduces a transient plateau or secondary phase in the occurrence rate and allows the model to reproduce sequences that do not follow a purely monotonic decay. In contrast to the classical ETAS formulation, this μ term should not be interpreted as an independent background rate, but rather as an internal component of the triggering process. This parametrization is consistent with the interpretation proposed by Godano et al. (2023), where the combined effect of impulsive stress perturbations and time-dependent relaxation processes (e.g., fluid dif-

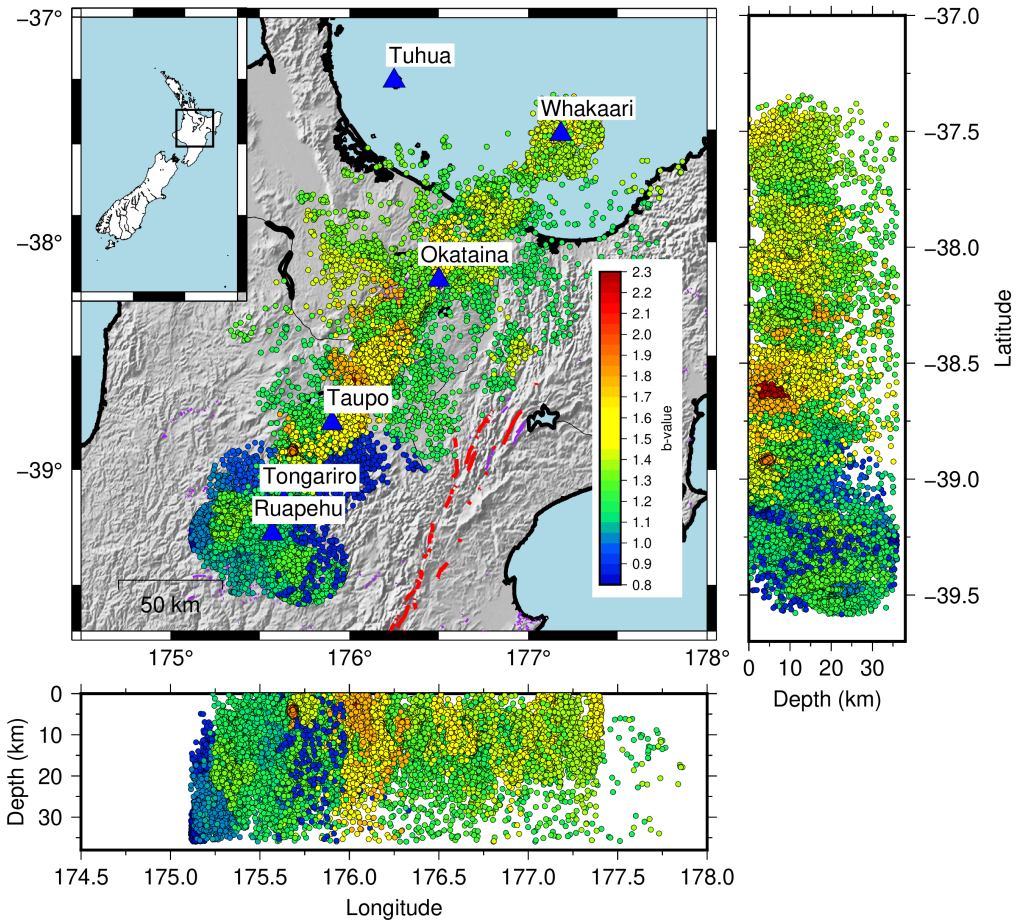

Figure 4 Spatial distribution of the Gutenberg-Richter b-value across the Taupō Volcanic Zone (TVZ), obtained using the CUBIT algorithm. Each cell contains at least 500 events and the b-value is estimated via the b-more-positive method. The map highlights clear spatial variability: higher b-values are concentrated in the younger volcanic centers (Whakaari and Taupō), while lower values are found beneath the older volcanoes (Tongariro and Ruapehu), consistent with increased stress in colder crustal volumes.

fusion or viscoelastic response) leads to a rate evolution characterized by an initial rapid decay followed by a finite-duration activation. As a result, the model is particularly suitable for describing swarm-like seismicity in volcanic calderas, where fluid and magma-related processes modulate the stress field independently of tectonic loading.

Within this framework, the term ”swarm-like” refers to temporal clustering patterns characterized by the absence of a dominant mainshock, repeated short-lived increases in seismicity rate, and a finite-duration memory. These features are consistent with the phenomenology of volcanic swarms described in the literature. In the present study, we apply this swarm-informed ETAS model to seismicity recorded in the Taupō Volcanic Zone (TVZ), New Zealand. The TVZ is a highly active region characterized by persistent and intense swarm activity, often associated with caldera dynamics and hydrothermal circulation. The goal is to assess whether the new kernel formulation improves the fit to the observed temporal clustering and provides physical insights into the underlying driving mechanisms.

Relation to alternative ETAS triggering kernel The development of alternative triggering kernels within the ETAS framework has a long history, motivated by the need to better represent deviations from the classical Omori-Utsu temporal decay and to improve the description of seismicity rates in different contexts (e.g., Mignan, 2015; Hainzl and Christophersen, 2017). These efforts include modifications of the temporal memory, departures from pure power-law decay, and physically motivated relaxations, often aimed at capturing features that the standard Omori kernel cannot reproduce. Within this broader context, the kernel adopted here is specifically tailored to swarm-dominated volcanic seismicity. Rather than proposing a universal replacement of the Omori-Utsu law, our goal is to model a well-defined class of sequences characterized by finite-duration activation and the absence of a dominant mainshock. The short-time behavior remains controlled by the exponent p, while the exponential taper introduces a finite characteristic timescale τ that naturally limits the memory of triggering, consistent with the finite duration of swarm episodes. This regime-specific formulation is motivated by the empirical scaling identified for volcanic swarms by Godano et al. (2023), and it provides a parsimonious extension of

ETAS that remains compatible with standard likelihood-based inference and operational forecasting workflows.

3.1 Parameter Estimation and Optimization

The parameters of the swarm-informed ETAS model are estimated by maximizing the conditional log-likelihood of the observed event times. The full parameter vector is

$$\theta = (\tau, p, \mu, K, \alpha),$$

where τ, p, and μ control the temporal shape of the triggering kernel, while K and α govern the productivity and its magnitude dependence.

Let $\{t_i\}_{i=1}^{N}$ denote the event times (in days) observed over the interval $[T_1, T_N]$. The log-likelihood function is defined as

$$\mathcal{L}(\theta) = \sum_{i=2}^{N} \ln\big[\lambda(t_i \mid \mathcal{H}_{t_i}; \theta)\big] \; - \; \int_{T_1}^{T_N} \lambda(t \mid \mathcal{H}_t; \theta)\, \mathrm{d}t, \quad (8)$$

where $\mathcal{H}_t$ denotes the history of events prior to time t, and the conditional intensity is given by

$$\lambda(t \mid \mathcal{H}_t; \theta) = \sum_{t_i < t} K\, e^{\alpha(m_i - M_0)} \times \frac{e^{-(t-t_i)/\tau}\left[\mu + (t-t_i)^{-p}\right]}{Z(\tau, p, \mu)}, \quad (9)$$

with the normalization constant

$$Z(\tau, p, \mu) = \mu\, \tau + \tau^{\,1-p}\, \Gamma(1-p).$$

Optimization procedure. Parameter estimation is performed by minimizing the negative log-likelihood $-\mathcal{L}(\theta)$ using a quasi-Newton algorithm (L-BFGS-B), which exploits both first-order gradients and an approximation of the local curvature of the objective function to ensure stable and efficient convergence.

The following bounds are imposed during optimization:

$$\tau > 0, \quad 0 < p < 1, \quad \mu \geq 0, \quad K > 0, \quad \alpha > 0.$$

In practice, we use

$$\begin{aligned} \tau &\in [10^{-9}, \infty), \\ p &\in [10^{-2}, 0.99], \\ \mu &\in [10^{-9}, \infty), \\ K &\in [10^{-9}, \infty), \\ \alpha &\in [10^{-9}, \infty). \end{aligned}$$

with initial guesses $\tau_0 = 1.0$ day, $p_0 = 0.5$, $\mu_0 = 0.1$, $K_0 = 0.1$, and $\alpha_0 = 1.0$. Convergence is declared when both the relative change in the objective function and the maximum absolute gradient component fall below 10^{-6}. Note that the admissible range of the exponent p differs between the stationary and swarm-informed ETAS formulations. In the classical ETAS model, $p > 1$ is required to ensure kernel normalizability, whereas in the swarm-informed model the exponential taper guarantees convergence even for $0 < p < 1$, allowing for short-lived, non-Omori-type clustering typical of volcanic swarms.

Model selection and goodness-of-fit We assess model performance using the Akaike Information Criterion (AIC), defined as $\mathrm{AIC} = 2k - 2\mathcal{L}(\widehat{\theta})$, where $k = 5$ is the number of fitted parameters. A lower AIC indicates a better trade-off between goodness of fit and model complexity.

To evaluate the benefits of the swarm-informed kernel, we also fitted the classical ETAS model (Eq. (3)) to the same dataset, using identical optimization procedures and convergence criteria. Table 1 compares the resulting AIC values.

Parameter uncertainties Formal uncertainties of the ETAS parameters are estimated from the local curvature of the log-likelihood function at the optimum. Specifically, we compute a numerical approximation of the Hessian matrix of the negative log-likelihood evaluated at the maximum-likelihood solution. Assuming local asymptotic normality of the estimator, the inverse Hessian provides an estimate of the covariance matrix of the parameters, and the reported uncertainties correspond to one standard deviation. This approach is commonly adopted in ETAS studies when the likelihood surface is sufficiently regular (e.g., Wang et al., 2010).

The swarm-informed model yields a significantly lower AIC value, supporting the idea that the inclusion of a finite memory timescale and an intermediate-rate plateau provides a more accurate representation of swarm dynamics in the TVZ.

The fitting improvement is quantified by $\Delta\mathrm{AIC} = 671.9$ (classical minus swarm-informed), which is far above the conventional threshold $\Delta\mathrm{AIC} > 10$ indicating decisive support for the better model. In terms of Akaike weights, this corresponds to an evidence ratio $\exp(\Delta\mathrm{AIC}/2) \approx 10^{146}$, i.e., essentially all the weight is assigned to the swarm-informed formulation within numerical precision.

Although Table 1 reports the optimized parameters for both models, it is important to stress that the parameterizations are not directly comparable one to one. In particular, the parameter μ has a fundamentally different meaning in the two formulations. In the classical ETAS model, μ represents a background seismicity rate, independent of the triggering process. In contrast, in the swarm-informed ETAS model, μ enters the triggering kernel itself and controls the balance between a quasi-stationary and a burst-like regime of seismic activity. Therefore, the larger numerical value of μ in the swarm-informed model does not indicate a higher background rate, but rather reflects a different internal decomposition of the seismicity rate. Direct comparison between models should thus focus on global measures such as likelihood or AIC, rather than on individual parameter values.

3.2 Results: Temporal Evolution of Seismic Rate

Figure 2 shows the temporal evolution of the seismic occurrence rate $\lambda(t)$ estimated from the swarm-informed ETAS model (Eq. (5)), together with the observed earthquake magnitudes. The inferred rate high-

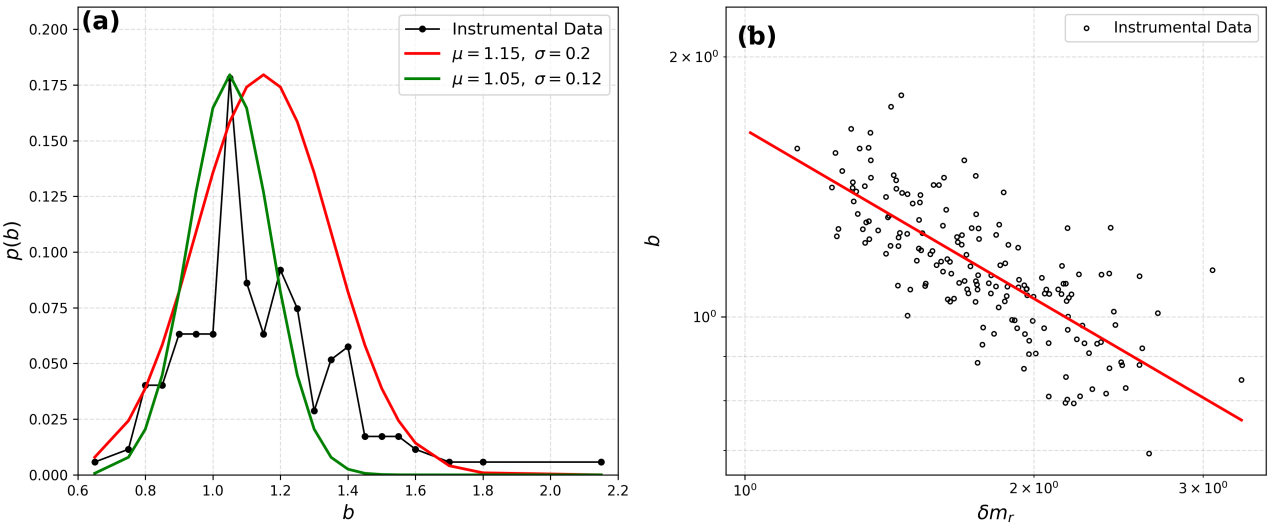

Figure 5 (a) The distribution of the b-values obtained for the 174 cells. The red and green curves are Gaussian distributions of parameters reported in the figure labels plotted as a guide for the eyes. (b) b-value as a function of δm_r. The red curve is a power law fit.

Model	K	α	c / τ (days)	p	μ (events/day)	AIC
Classical ETAS	0.40 ± 0.04	0.71 ± 0.07	$7.6 \times 10^{-3} \pm 1.4 \times 10^{-4}$	1.09 ± 0.03	$1.1 \times 10^{-4} \pm 6.5 \times 10^{-5}$	2818.75
Swarm-informed ETAS	4.29 ± 0.76	1.85 ± 0.09	100.02 ± 13.4	0.96 ± 0.01	0.036 ± 0.007	2146.89

Table 1 Optimized parameters and AIC for the classical and swarm-informed ETAS models. For the classical ETAS, the parameter c appears in the Omori kernel; for the swarm-informed ETAS, c is replaced by the exponential cutoff timescale τ.

lights a strongly nonstationary behavior, characterized by alternating phases of enhanced seismic activity and relative quiescence, which are typical of volcanic and geothermal regions dominated by swarm-like seismicity. At short timescales, the model captures rapid increases in seismic rate followed by progressive decays, reflecting the finite duration nature of individual swarm episodes. These rate transients are not consistent with classical mainshock-aftershock sequences (Lippiello et al., 2019; Petrillo et al., 2020; Lippiello et al., 2021), but rather indicate repeated episodes of fluid or magma driven activation, in agreement with the geological and geothermal setting of the Taupō Volcanic Zone. At longer timescales, the estimated rate exhibits a gradual decay between approximately 800 and 3000 days after the beginning of the catalog. This trend does not show a clear periodic or seasonal modulation and is therefore unlikely to reflect environmental forcing or catalog artifacts. Instead, it is interpreted as the cumulative effect of a progressive reduction in swarm productivity, possibly associated with the relaxation of transient magmatic or hydrothermal processes active during the earlier phase of the catalog. Importantly, the long-term decay of $\lambda(t)$ coincides with a decrease in the frequency of large swarm episodes rather than with a systematic change in background seismicity. This suggests that the observed rate variations primarily reflect changes in swarm occurrence and intensity, rather than variations in the tectonic loading rate. The temporal evolution of the seismic rate is used to identify distinct phases of seismic activity, which can be associated with different regions of the Taupō Volcanic Zone and subsequently analyzed in terms of their b-value variations. Periods of elevated seismic rate correspond to swarm-dominated phases, during which magnitude statistics are expected to be more strongly influenced by fluid-driven stress heterogeneity. This motivates the joint analysis of seismic rate and b-value variations as complementary diagnostics of the underlying physical processes in the TVZ.

Link to documented unrest During the study period, a number of volcanic eruptions affected the TVZ. Early in the catalogue, the 25 September 2007 eruption of Ruapehu was a moderate, gas-driven event that produced ballistic ejecta and a fallout apron (Kilgour et al., 2010). This was followed by the 6 August and 21 November 2012 eruptions of Tongariro, both explosive events accompanied by substantial ash plumes (Leonard et al., 2021). Later, on 9 December 2019, Whakaari experienced a phreatic eruption characterized by the rapid release of steam and volcanic gases, generating an explosion and widespread ballistic and lithic fallout (Cas, 2025). A prominent seismic rate enhancement occurs at ~ 2018.75 (approximately Sep 2018), which coincides with the beginning of 2019 unrest at Taupō volcano documented by Illsley-Kemp et al. (2021). That episode consisted of multiple swarms over several months and was accompanied by measurable GNSS deformation interpreted as pressurization/intrusion at $\sim$ 58 km depth. The fact that this unrest is expressed in our catalog primarily as repeated rate transients with finite duration supports the use of a swarm-informed triggering kernel consistent with the non-aftershock nature of the se-

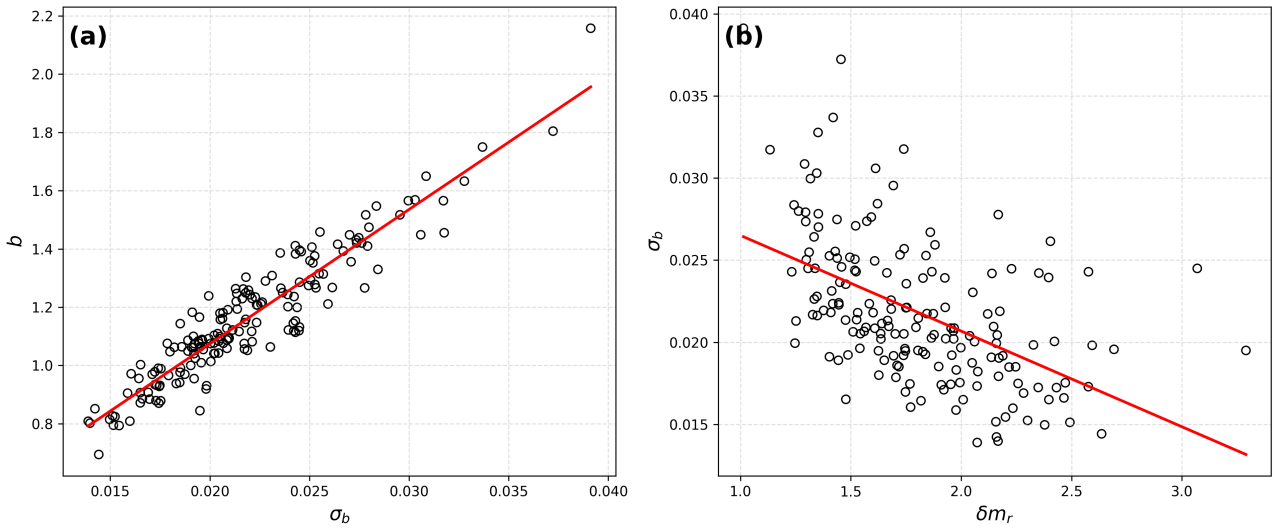

Figure 6 (a) b-value as a function of the corresponding standard error σ_b across the volcanic system. b-value is estimated in each cell using the b-more-positive method. (b) The corresponding standard error σ_b as a function of the magnitude range for each cell.

quence reported in that study.

Maximum magnitude Over the 17-year interval we also observe an increase of the maximum recorded magnitude toward the end of the catalog (including the recent $M_L \sim 4.5$ event). Given the strong clustering and intermittency typical of TVZ seismicity, we interpret this as reflecting the episodic occurrence of larger swarm episodes rather than a systematic change in background tectonic loading; a dedicated physical attribution would require joint interpretation with geodetic and volcanic monitoring data.

Comparison with a nonstationary ETAS and goodness-of-fit diagnostics. To benchmark the proposed swarm-informed ETAS against a standard nonstationary ETAS, we also fitted the non-stationary background formulation of the ETAS model (Kumazawa and Ogata, 2014), in which the background rate and productivity vary smoothly in time and are estimated by penalized maximum likelihood, with the smoothing strength selected by ABIC. Specifically, we parameterized: $\mu(t) = \mu_{\text{ref}}\, q_\mu(t)$, $K_0(t) = K_{0,\text{ref}}\, q_{K_0}(t)$, where $q_\mu(t) = \exp[s_\mu(t)]$ and $q_{K_0}(t) = \exp[s_{K_0}(t)]$, with $s_\mu(t)$ and $s_{K_0}(t)$ represented by cubic splines. This log-spline formulation ensures positivity while allowing flexible temporal variability. In the implementation adopted here, no change point was introduced, and each spline was defined using 8 uniformly spaced knots over the observation window. The parameters were estimated by maximizing a penalized log-likelihood function. The roughness penalty was applied to the spline coefficients through the sum of squared first differences, thereby discouraging unrealistically rapid temporal oscillations in $q_\mu(t)$ and $q_{K_0}(t)$. The smoothing strength w was selected by minimizing the ABIC. In practice, we explored a discrete set of candidate values $w \in \{0.0, 0.01, 0.05, 0.1, 0.3, 1.0\}$, and for each value we performed a full likelihood optimization. The optimal model corresponds to $\text{ABIC} = 520.30$.

The nonstationary ETAS model remains a highly flexible time-dependent formulation characterized by a large number of spline coefficients. Therefore, its effective model complexity is not directly comparable to that of the stationary or swarm-informed ETAS models, and a standard AIC-based comparison is not appropriate. For this reason, we assess model performance consistently across all formulations using the transformed time

$$\tau_i = \int_{T_1}^{t_i} \lambda(u \mid \mathcal{H}_u)\, du. \tag{10}$$

A correctly specified conditional intensity yields a unit-rate Poisson process in τ. We therefore compare $N(\tau)$ to the expected diagonal $N(\tau) = \tau$, which provides a consistent diagnostic across stationary, swarm-informed, and nonstationary ETAS formulations (Fig.3).

4 The b-value variations

4.1 Results: The b-value mapping

To perform the b-value mapping we use the CUBIT algorithm. Firstly, the algorithm was introduced by Godano et al. (2022a) and then applied to characterize the stress state on the Antakya fault (Convertito et al., 2024a), on the faults of the major ($m > 7$) Californian earthquakes Convertito et al. (2024b), in the volcanic area of Campi Flegrei (Convertito et al., 2025) and in other volcanic areas of the world (Godano et al., 2024b). The algorithm finds the largest event in the catalogue not yet assigned to a cell and includes in the cell all earthquakes close to the selected one until when the number of events in the cell reaches the value $n \pm n_{tol}$. This choice could appear inappropriate because volcanic earthquakes swarms are not controlled by the occurrence of a mainshock. However, it is still possible to define a productivity law governed by the largest event in the swarm. This implies that the mechanism con-

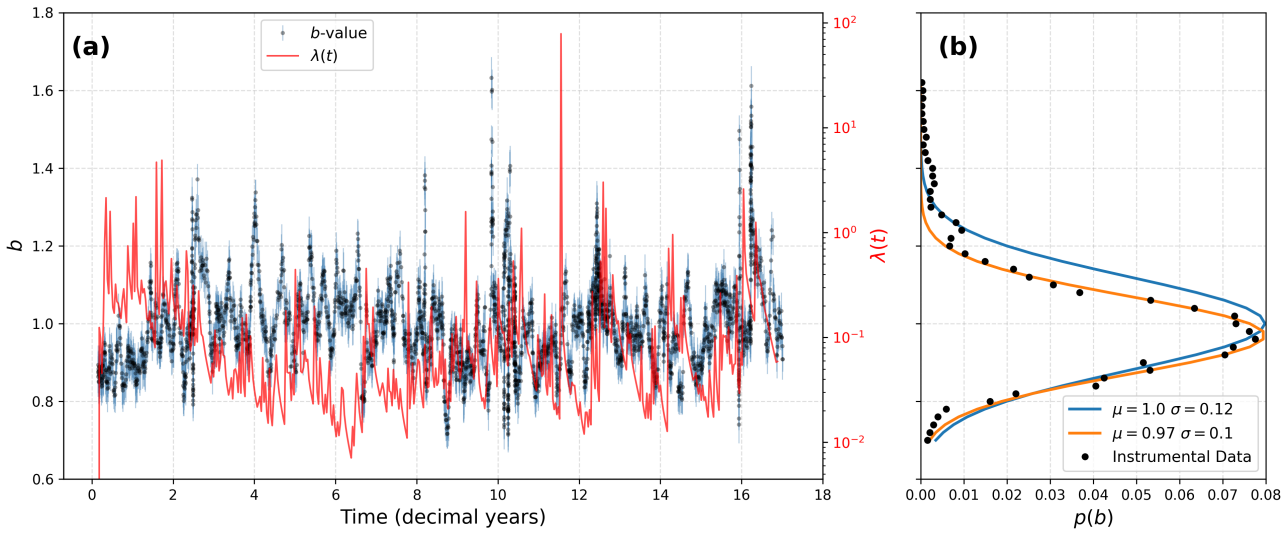

Figure 7 Temporal evolution of the b-value estimated using the b-more-positive method (black dots, with uncertainty bars), shown together with the seismic occurrence rate $\lambda(t)$ inferred from the swarm-informed ETAS model (red curve, right axis). Time is expressed in decimal years. Displaying both quantities on the same time axis facilitates a direct visual comparison between variations in seismic rate and fluctuations in the magnitude distribution. (b) Empirical probability density function p(b) of the observed b-values (black dots), compared with two theoretical distributions (solid lines) characterized by different mean μ and standard deviation σ

trolling swarm occurrence (most likely crustal deformation) also controls the magnitude of the largest event within the swarm. Here n=500 and n_{tol}=50.

Then, the b-value in each cell is estimated using the b-more-positive method (Lippiello and Petrillo, 2024). The method is based on the statistical distribution of positive magnitude differences $\delta m = m_j - m_i$ between pairs of earthquakes, which follows an exponential law with slope controlled by the b-value. In contrast to the original b-positive formulation (van der Elst, 2021a), which considers only consecutive event pairs, the b-more-positive method allows for non-consecutive pairs provided that the two events are separated by less than a prescribed spatial distance. This spatial constraint ensures that both earthquakes are subject to comparable local detection conditions, under the assumption that completeness varies smoothly in space (Lippiello and Petrillo, 2024). As a result, the method mitigates spatial incompleteness effects without requiring an explicit estimate of the magnitude of completeness. Lippiello and Petrillo (2024) further demonstrated that reliable estimation requires introducing a minimum magnitude increment threshold δm_{th}, and excluding pairs with $\delta m < \delta m_{th}$. Small magnitude differences are preferentially affected by detection incompleteness and lead to a systematic underestimation of b when included. By retaining only $\delta m \geq \delta m_{th}$, the estimator effectively isolates magnitude differences for which the conditional detection probability is close to unity, yielding stable and asymptotically unbiased b estimates. Recently, this framework has been further generalized into an unsupervised likelihood-based approach that jointly estimates the b-value and incompleteness effects directly from magnitude differences (Godano et al., 2025a). In this study, we adopt a uniform threshold $\delta m_{th} = 0.5$ for all cells, which provides stable estimates across the Taupō Volcanic Zone and ensures consistency in the comparison of spatial b-value variations.

Figure 4 shows the map obtained for the TVZ earthquake catalogue. The algorithm creates 174 cell with b-values $\in [0.75, 2.26]$ and an estimation error (evaluated following Shi and Bolt, 1982) $\sigma_b \in [0.014, 0.039]$. The distribution of the b-value appears to be close to a Gaussian one (Fig. 5). However, using the average b, 1.15 and its standard deviation, 0.2 the gaussian distribution appears to be a very bad fit of the experimental curve. In fact, the skewness of the distribution is 0.8. The fit, obtained removing the tail for $b > 1.35$, greatly improves using $\langle b \rangle$=1.05 and a standard deviation σ=0.12.

The presence of the skewed data could be explained by a correlation between the b-value and the range of the magnitude differences δm_r (Figure 5). The red line represents the power law $b = 1.65 \delta m_r^{-0.65}$ with a χ^2=0.015. The presence of such a correlation suggests that the b-value is dependent on the estimation error as shown in Figure 6(a). The very poor correlation between σ_b and δm_r (Figure 6b) represents an indication that the correlation showed in Figure 5b is not an artifact due to the dependence of b on σ_b, but a significant relationship between b and the stress (when the earthquakes are small the b-value is higher and the stress smaller).

Figure 4 shows as the higher b-values are observed for Whakaairi and Taupō volcanoes which are the younger ones. On the contrary, the oldest volcanoes (Tongariro and Ruapehu) exhibit the smaller b-values. Despite its old constructional age, Ōkataina remains an active magmatic system characterized by significant heat and fluid circulation, which can maintain elevated or intermediate b-values independent of its long-term volcanic history. This is in full agreement with what observed for other volcanoes of the world (Godano et al., 2024b) and confirms that the colder rocks of the older volcanoes

can support larger stress in respect of the younger ones where the temperature is higher.

4.2 Results: The b-value time variations

The temporal variations of the b-value were investigated by estimating b in sliding windows of 500 earthquakes, shifted one event at a time. As in the spatial analysis, the b estimate was performed using the b-more-positive method (Lippiello and Petrillo, 2024), with a threshold $\delta m_{th} = 0.5$. This procedure yields 86 079 b-value estimates spanning the interval $[0.7, 1.6]$. The associated uncertainties, evaluated following Shi and Bolt (1982), range between 10^{-2} and 6×10^{-2}. The resulting distribution is approximately Gaussian (Fig. 7b), although a slight positive skewness is observed ($\gamma = 0.18$). As in the spatial case, a fit using $\langle b \rangle = 1.0$ and $\sigma = 0.12$ provides a poorer description than a fit with $\langle b \rangle = 0.97$ and $\sigma = 0.10$ (obtained removing the tail distribution for $b > 1.35$), which better captures the central tendency of the data. This discrepancy is attributed to the residual skewness of the distribution, although it is weaker than in the spatial analysis.

The temporal evolution of the b-value is shown in Fig. 7a. The time series exhibits pronounced fluctuations, with variations that locally exceed the estimated uncertainty range, indicating that the observed variability cannot be attributed to statistical noise alone. Importantly, the temporal evolution of the b-value shows a co-variation with the seismic occurrence rate, with periods of increased seismic activity often accompanied by noticeable changes in the magnitude distribution. Periods of enhanced seismic rate, associated with swarm-like activity, tend to coincide with increased variability and locally elevated b-values, whereas more quiescent intervals are characterized by more stable b estimates. This behavior suggests that both the seismic rate and the b-value respond to the same underlying physical processes, likely related to transient fluid or magma migration and the resulting stress heterogeneity. In this framework, elevated b-values reflect a dominance of distributed microfracturing and fluid-assisted rupture, while lower and more stable b-values are indicative of comparatively more homogeneous stress conditions.

As in the spatial analysis, the slight skewness of the b-value distribution can be related to the correlation between b and the magnitude increment δm_r (Fig. 8a). However, in the temporal case the power-law fit is significantly poorer (Fig. 8), suggesting that this coupling is weaker or more intermittent in time than in space. This difference highlights a fundamental distinction between spatial and temporal analyses. Spatial correlations may reflect persistent structural and thermo-mechanical heterogeneities of the crust, such as variations in lithology, temperature, and long-lived fluid pathways, which can sustain a stable relationship between magnitude statistics and rupture increments. In contrast, temporal variations are governed by transient processes, including episodic fluid or magma migration and short-lived stress perturbations, which may intermittently modify the magnitude distribution without establishing a robust scaling relation. Finally, no correlation is observed between b and its associated uncertainty σ_b (Fig. 8b), confirming that the observed temporal variability of b is not driven by changes in estimation precision.

5 Implications for forecasting volcanic seismicity

This study does not aim to develop a forecasting model for volcanic unrest. Instead, it focuses on the characterization of seismic regimes through the joint analysis of seismicity rate and b-value variations. Within this framework, it is important to distinguish between:

- the seismicity rate, which can be modeled within an ETAS-type framework and used for probabilistic forecasting of earthquake occurrence,
- the b-value, which reflects the statistical distribution of magnitudes and provides insight into the physical state of the system.

From an interpretative perspective, the joint analysis of seismicity rate and b-value variations provides complementary information on the evolving seismic regime. Periods of elevated seismic rate combined with enhanced b-value variability are indicative of swarm-dominated, fluid-driven activity, whereas more stable b-values and lower rates suggest comparatively homogeneous stress conditions (Godano et al., 2024b). We emphasize that these observations should be interpreted as diagnostic indicators rather than as direct forecasting tools. In particular, b-value variations are not used here as predictive variables, but as proxies for the underlying thermo-mechanical state of the volcanic system. A quantitative assessment of their predictive capability would require a dedicated validation framework (e.g., prospective testing or retrospective skill evaluation), which is beyond the scope of the present study. Nevertheless, the proposed framework suggests a promising direction for integrating statistical and physical indicators in future volcanic unrest forecasting models.

6 Conclusions

In this work, we have analyzed the seismicity of the Taupō Volcanic Zone by integrating a swarm-informed ETAS model with a high-resolution b-value mapping, offering a combined perspective on the temporal and magnitude clustering of earthquakes in a volcanic setting.

We present a modified ETAS model incorporating a kernel inspired by the Gamma distribution proposed by Godano et al. (2023), which captures the finite duration and complex triggering dynamics of seismic swarms. This swarm-informed model significantly improves the fit to TVZ seismicity compared to the classical ETAS formulation, as evidenced by a substantial reduction in AIC. The model provides a more realistic description of volcanic swarm activity by accounting for a finite memory timescale.

In parallel, we performed a spatial and temporal analysis of the Gutenberg-Richter b-value using the CUBIT

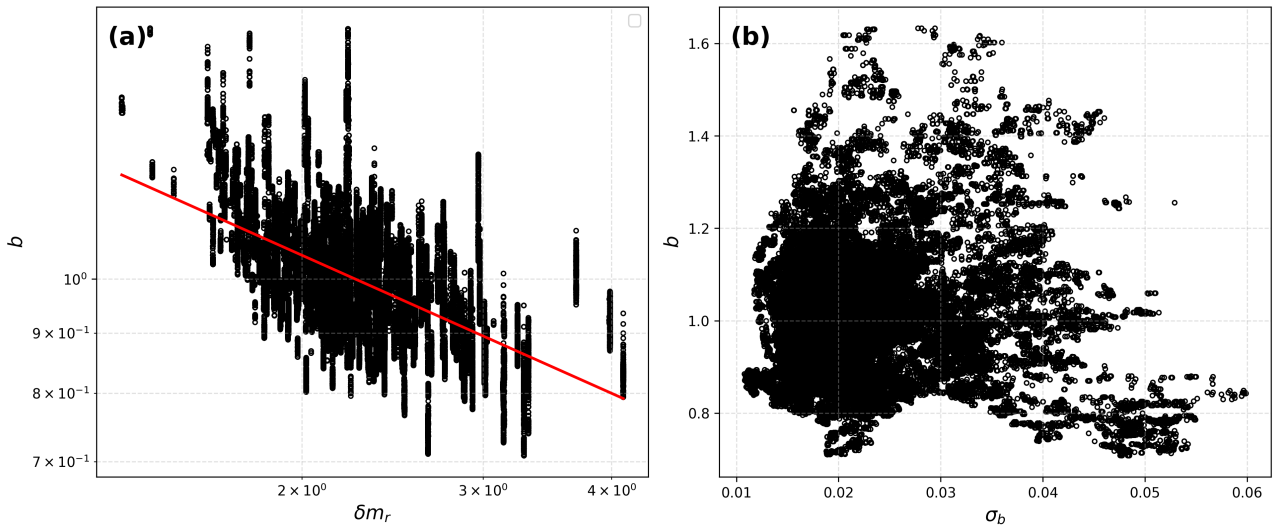

Figure 8 (a) Relationship between the b-value estimated in each time window and the magnitude increment range δm_r. The red curve represents the power-law fit. (b) Relationship between the b-value and its associated standard error σ_b in each time window.

algorithm and the b-more-positive estimation method. Our results reveal a clear spatial pattern: higher b-values are associated with the younger, hotter volcanic centers (Whakaari and Taupō), while older volcanoes (Tongariro and Ruapehu) exhibit lower b-values. This is consistent with previous results obtained for other volcanoes of the world (Godano et al., 2024b). The distribution of b-values across space and time displays a slight positive skewness, which we interpret as the result of a correlation between b and the local magnitude range δm_r. This highlights the genuine relationship between b-values and the stress state: when earthquakes are smaller (small δm_r) b assumes larger values.

Altogether, this study underscores the necessity of using physically informed point-process models and robust statistical tools when analyzing complex volcanic seismicity. Future work could explore the incorporation of additional geophysical observables (e.g., deformation, fluid migration) into the swarm kernel and extend the b-value analysis to include real-time monitoring and forecasting applications.

Acknowledgements

We thank the reviewers, M. Laporte and M.-S. Seo, for their careful reading of the manuscript and for their constructive comments, which helped improve the clarity and quality of this work. The publication was produced with the co-financing of the European Union - Next Generation EU. This publication has been supported by the project titled D.I.R.E.C.T.I.O.N.S. - Deep learning aIded foReshock deteCTIOn Of iNduced mainShocks, project code: P20220KB4F, CUP: E53D23032910001, PRIN 2022 - Piano Nazionale di Ripresa e Resilienza (PNRR), Mission 4 “Istruzione e Ricerca” - Componente C2 Investimento 1.1, “Fondo per il Programma Nazionale di Ricerca e Progetti di Rilevante Interesse Nazionale (PRIN).” C. G. acknowledges MUR project PRIN 2022 PNRR P20222B5P9 for partial financial support.

Data and code availability

The earthquake catalogue is freely available at https://doi.org/10.5281/zenodo.13138604. Code is available at https://doi.org/10.5281/zenodo.16439643.

Competing interests

The authors have no competing interests.

References

Amitrano, D. Brittle-ductile transition and associated seismicity: Experimental and numerical studies and relationship with the b value. *Journal of Geophysical Research: Solid Earth*, 108(B1): 2044, 2003. doi: 10.1029/2001JB000680.

Barker, S. J., Wilson, C. J., Illsley-Kemp, F., Leonard, G. S., Mestel, E. R., Mauriohooho, K., and Charlier, B. L. Taupō: an overview of New Zealand’s youngest supervolcano. *New Zealand Journal of Geology and Geophysics*, 64(2-3):320–346, 2021. doi: 10.1080/00288306.2020.1792515.

Bridges, D. L. and Gao, S. S. Spatial variation of seismic b-values beneath Makushin Volcano, Unalaska Island, Alaska. *Earth and Planetary Science Letters*, 245(1–2):408 – 415, 2006. doi: 10.1016/j.epsl.2006.03.010.

Cas, R. A. The fatal 9th December 2019 eruption disaster on Whakaari/White Island volcano, New Zealand: Contributing factors, failures, and lessons for volcano tourism. *Journal of Volcanology and Geothermal Research*, page 108461, 2025. doi: 10.1016/j.jvolgeores.2025.108461.

Chiba, K. and Shimizu, H. Spatial and temporal distributions of b-value in and around Shinmoe-dake, Kirishima volcano, Japan. *earth, planets and space*, 70(1):1–9, 2018. doi: 10.1186/s40623-018-0892-7.

Cole, J., Thordarson, T., and Burt, R. Magma origin and evolution of White Island (Whakaari) volcano, Bay of plenty, New Zealand. *Journal of Petrology*, 41(6):867–895, 2000. doi: 10.1093/petrology/41.6.867.

Collettini, C., Barchi, M. R., De Paola, N., Trippetta, F., and Tinti, E. Rock and fault rheology explain differences between on fault and distributed seismicity. *Nature communications*, 13(1):5627, 2022. doi: 10.1038/s41467-022-33373-y.

Convertito, V., Tramelli, A., and Godano, C. b map evaluation and on-fault stress state for the Antakya 2023 earthquake. *Scientific Reports*, 2024a. doi: 10.1038/s41598-023-50837-3.

Convertito, V., Tramelli, A., and Godano, C. Evaluation of the b Maps on the Faults of the Major (M> 7) South California Earthquakes. *Earth and Space Science*, 11(6):e2023EA002933, 2024b. doi: 10.1029/2023ea002933.

Convertito, V., Godano, C., Petrillo, G., and Tramelli, A. Insights from b value analysis of Campi Flegrei unrests. *Scientific Reports*, 15(1):14974, 2025. doi: 10.1038/s41598-025-98240-4.

D., S., S., W., and M, W. Variations in earthquake-size distribution across different stress regimes. *Nature*, 437, 2005. doi: 10.1038/nature04094.

Farrell, J., Husen, S., and Smith, R. B. Earthquake swarm and b-value characterization of the Yellowstone volcano-tectonic system. *Journal of Volcanology and Geothermal Research*, 188(1-3): 260–276, 2009. doi: 10.1016/j.jvolgeores.2009.08.008.

Gentili, S., Brondi, P., Rossi, G., Sugan, M., Petrillo, G., Zhuang, J., and Campanella, S. Seismic clusters and fluids diffusion: a lesson from the 2018 Molise (Southern Italy) earthquake sequence. *Earth, Planets and Space*, 76(1):157, 2024. doi: 10.1186/s40623-024-02096-3.

Godano, C., Convertito, V., Pino, N. A., and Tramelli, A. An Automated Method for Mapping Independent Spatial b Values. *Earth and Space Science*, 9(6):e2021EA002205, 2022a. doi: 10.1029/2021EA002205.

Godano, C., Tramelli, A., Petrillo, G., Bellucci Sessa, E., and Lippiello, E. The dependence on the Moho depth of the b-value of the Gutenberg–Richter law. *Bulletin of the Seismological Society of America*, 112(4):1921–1934, 2022b. doi: 10.1785/0120210144.

Godano, C., Tramelli, A., Mora, M., Taylor, W., and Petrillo, G. An analytic expression for the volcanic seismic swarms occurrence rate. A case study of some volcanoes in the world. *Earth and Space Science*, 10(2):e2022EA002534, 2023. doi: 10.1029/2022ea002534.

Godano, C., Petrillo, G., and Lippiello, E. Evaluating the incompleteness magnitude using an unbiased estimate of the b value. *Geophysical Journal International*, 236(2):994–1001, 2024a. doi: 10.1093/gji/ggad466.

Godano, C., Tramelli, A., Papadimitriou, E., Karakostas, V., Petrillo, G., and Convertito, V. b-Value Maps for Some Volcanoes Worldwide: What Do We Learn? *Seismological Research Letters*, 95(6): 3557–3565, 2024b. doi: 10.1785/0220240204.

Godano, C., Tramelli, A., Petrillo, G., and Convertito, V. Testing the Predictive Power of b Value for Italian Seismicity. *Seismica*, 3(1), 2024c. doi: 10.26443/seismica.v3i1.1084.

Godano, C., Lippiello, E., and Petrillo, G. Unsupervised Likelihood Inference of the b-Value via Magnitude Differences. *Journal of Geophysical Research: Machine Learning and Computation*, 2(4): e2025JH000863, 2025a. doi: 10.1029/2025JH000863.

Godano, C., Petrillo, G., Tramelli, A., and Convertito, V. The b-Value Tomography of the Calabrian Arc. *Earth and Space Science*, 12(6):e2024EA004065, 2025b. doi: 10.1029/2024EA004065.

Gulia, L. and Wiemer, S. The influence of tectonic regimes on the earthquake size distribution: A case study for Italy. *Geophysical Research Letters*, 37(10), 2010. doi: 10.1029/2010GL043066.

Gulia, L. and Wiemer, S. Real-time discrimination of earthquake foreshocks and aftershocks. *Nature*, 574:193–199, 2019. doi: 10.1038/s41586-019-1606-4.

Gulia, L., Rinaldi, A. P., Tormann, T., Vannucci, G., Enescu, B., and Wiemer, S. The Effect of a Mainshock on the Size Distribution of the Aftershocks. *Geophysical Research Letters*, 45(24): 13,277–13,287, 2018. doi: 10.1029/2018GL080619.

Gulia, L., Wiemer, S., and Vannucci, G. Pseudoprospective Evaluation of the Foreshock Traffic-Light System in Ridgecrest and Implications for Aftershock Hazard Assessment. *Seismological Research Letters*, 91:2828—2842, 2020. doi: 10.1785/0220190307.

Gutenberg, B. and Richter, C. Frequency of earthquakes in California. *Bulletin of the Seismological Society of America*, 34(4): 185–188, 1944. doi: 10.1785/bssa0340040185.

Hainzl, S. and Christophersen, A. Testing alternative temporal aftershock decay functions in an ETAS framework. *Geophysical Journal International*, 210(2):585–593, 2017. doi: 10.1093/gji/ggx184.

Helmstetter, A. Is Earthquake Triggering Driven by Small Earthquakes? *Phys. Rev. Lett*, 91:058501, Jul, 2003. doi: 10.1103/PhysRevLett.91.058501.

Illsley-Kemp, F. and Mestel, E. A new consistent and high-precision earthquake catalogue for the Taupō Volcanic Zone, New Zealand. *Seismica*, 4(1), 2025. doi: 10.26443/seismica.v4i1.1490.

Illsley-Kemp, F., Barker, S. J., Wilson, C. J., Chamberlain, C. J., Hreinsdóttir, S., Ellis, S., Hamling, I. J., Savage, M. K., Mestel, E. R., and Wadsworth, F. B. Volcanic unrest at Taupō volcano in 2019: Causes, mechanisms and implications. *Geochemistry, Geophysics, Geosystems*, 22(6):e2021GC009803, 2021. doi: 10.1029/2021gc009803.

Jolly, A. D. and McNutt, S. R. Seismicity at the volcanoes of Katmai National Park, Alaska; July 1995–December 1997. *Journal of Volcanology and Geothermal Research*, 93(3-4):173–190, 1999. doi: 10.1016/s0377-0273(99)00115-8.

Kamer, Y. and Hiemer, S. Data-driven spatial b value estimation with applications to California seismicity: To b or not to b. *Journal of Geophysical Research: Solid Earth*, 120(7):5191–5214, 2015. doi: 10.1002/2014JB011510.

Kilgour, G., Manville, V., Della Pasqua, F., Graettinger, A., Hodgson, K., and Jolly, G. The 25 September 2007 eruption of Mount Ruapehu, New Zealand: directed ballistics, surtseyan jets, and ice-slurry lahars. *Journal of Volcanology and Geothermal Research*, 191(1-2):1–14, 2010. doi: 10.1016/j.jvolgeores.2009.10.015.

Knett, J. *Das Erzgebirgische Schwarmbeben zu Hartenberg vom 1. Jänner bis 5. Feber 1824*. Mercy, 1899.

Kumazawa, T. and Ogata, Y. Nonstationary ETAS models for nonstandard earthquakes. *The Annals of Applied Statistics*, 8(3): 1825, 2014. doi: 10.1214/14-aoas759.

Leonard, G. S., Cole, R. P., Christenson, B. W., Conway, C. E., Cronin, S. J., Gamble, J. A., Hurst, T., Kennedy, B. M., Miller, C. A., Procter, J. N., et al. Ruapehu and Tongariro stratovolcanoes: a review of current understanding. *New Zealand Journal of Geology and Geophysics*, 64(2-3):389–420, 2021. doi: 10.1080/00288306.2021.1909080.

Lippiello, E. and Petrillo, G. b-more-incomplete and b-more-positive: Insights on a robust estimator of magnitude distribution. *Journal of Geophysical Research: Solid Earth*, 129(2): e2023JB027849, 2024. doi: 10.1029/2023jb027849.

Lippiello, E., Petrillo, G., Landes, F., and Rosso, A. Fault Heterogeneity and the Connection between Aftershocks and Afterslip. *Bulletin of the Seismological Society of America*, 109(3): 1156–1163, 04, 2019. doi: 10.1785/0120180244.

Lippiello, E., Petrillo, G., Landes, F., and Rosso, A. The Genesis of Aftershocks in Spring Slider Models. *Statistical Meth-*

ods and Modeling of Seismogenesis, 1:131–151, 2021. doi: 10.1002/9781119825050.ch5.

Lippiello, E., Petrillo, G., Godano, C., and Dal Zilio, L. Toward Recognizing the Waveform of Foreshocks. *Geophysical Research Letters*, 52(15), 2025a. doi: 10.1029/2025gl115466.

Lippiello, E., Petrillo, G., Godano, C., Papadimitriou, E., Karakostas, V., and Anagnostou, V. 2025 Santorini-Amorgos crisis triggered by a transition from volcanic to regular tectonic activity. *arXiv preprint arXiv:2504.21371*, 2025b. doi: 10.48550/arXiv.2504.21371.

Liu, Y., Zhuang, J., Guo, Y., Jiang, C., Tian, Q., Zhang, Y., and Long, F. Background and clustering characteristics of recent seismicity in Southwestern China. *Geophysical Journal International*, 238 (3):1291–1313, 2024. doi: 10.1093/gji/ggae211.

Mesimeri, M., Kourouklas, C., Papadimitriou, E., Karakostas, V., and Kementzetzidou, D. Analysis of microseismicity associated with the 2017 seismic swarm near the Aegean coast of NW Turkey. *Acta Geophysica*, 66:479–495, 2018. doi: 10.1007/s11600-018-0157-7.

Mignan, A. Modeling aftershocks as a stretched exponential relaxation. *Geophysical Research Letters*, 42(22):9726–9732, 2015. doi: 10.1002/2015gl066232.

Miller, S. A., Collettini, C., Chiaraluce, L., Cocco, M., Barchi, M., and Kaus, B. J. Aftershocks driven by a high-pressure CO2 source at depth. *Nature*, 427(6976):724–727, 2004. doi: 10.1038/nature02251.

Mogi, K. Study of the elastic shocks caused by the fracture of heterogeneous materials and its relation to earthquake phenomena. *Bull. Earthq. Res. Inst. Tokyo Univ*, 40:125–173, 1962.

Morgenstern, R., Litchfield, N. J., Langridge, R. M., Heron, D. W., Townsend, D. B., Villamor, P., Barrell, D. J. A., Ries, W. F., Van Dissen, R. J., Clark, K. J., Coffey, G. L., Zoeller, A., Howell, A., and Easterbrook-Clarke, L. H. New Zealand Active Faults Database: the high-resolution dataset v2.0. *New Zealand Journal of Geology and Geophysics*, ahead-of-print(ahead-of-print):1–16, 2024. doi: 10.1080/00288306.2024.2427396.

Murru, M., Montuori, C., Wyss, M., and Privitera, E. The locations of magma chambers at Mt. Etna, Italy, mapped by b-values. *Geophysical research letters*, 26(16):2553–2556, 1999. doi: 10.1029/1999gl900568.

Murru, M., Console, R., Falcone, G., Montuori, C., and Sgroi, T. Spatial mapping of the b value at Mount Etna, Italy, using earthquake data recorded from 1999 to 2005. *Journal of Geophysical Research: Solid Earth*, 112(B12):n/a–n/a, 2007. doi: 10.1029/2006JB004791.

Ogata, Y. Statistical Models for Earthquake Occurrences and Residual Analysis for Point Processes. *Research Memo. (Technical report) Inst. Statist. Math., Tokyo*, 288, 1985.

Ogata, Y. Statistical Models for Earthquake Occurrences and Residual Analysis for Point Processes. *J. Amer. Statist. Assoc*, 83:9 – 27, 1988. doi: 10.1080/01621459.1988.10478560.

Ogata, Y. A Monte Carlo method for high dimensional integration. *Numerische Mathematik*, 55(2):137–157, 1989. doi: 10.1007/BF01406511.

Ogata, Y. Space-time point-process models for earthquake occurrences. *Annals of the Institute of Statistical Mathematics*, 50: 379–402, 1998. doi: 10.1023/a:1003403601725.

Omori, F. On the after-shocks of earthquakes. *J. Coll. Sci. Imp. Univ. Tokyo*, 7:111–200, 1894.

Oynakov, E., Aleksandrova, I., and Popova, M. Characteristics of the 2025 Santorini-Amorgos seismic swarm. *Geofizika*, 42(2): 1–18, 2025. doi: 10.15233/gfz.2025.42.6.

Papadopoulos, G. A., Charalampakis, M., Fokaefs, A., and Minadakis, G. Strong foreshock signal preceding the L'Aquila (Italy) earthquake (M_w 6.3) of 6 April 2009. *Natural Hazards and Earth System Science*, 10(1):19–24, 2010. doi: 10.5194/nhess-10-19-2010.

Papale, P. Global time-size distribution of volcanic eruptions on Earth. *Scientific reports*, 8(1):6838, 2018. doi: 10.1038/s41598-018-25286-y.

Petrillo, G. and Lippiello, E. Testing of the foreshock hypothesis within an epidemic like description of seismicity. *Geophysical Journal International*, 225(2):1236–1257, 2021. doi: 10.1093/gji/ggaa611.

Petrillo, G. and Lippiello, E. Incorporating foreshocks in an epidemic-like description of seismic occurrence in Italy. *Applied Sciences*, 13(8):4891, 2023. doi: 10.3390/app13084891.

Petrillo, G. and Taroni, M. Adding strain rate information into a short-term seismicity model improves forecasting performances: the case of Campi Flegrei, Italy. *Seismica*, 4(2), 2025. doi: 10.26443/seismica.v4i2.1908.

Petrillo, G. and Zhuang, J. Bayesian earthquake forecasting approach based on the epidemic type aftershock sequence model. *Earth, Planets and Space*, 76(1):78, 2024. doi: 10.1186/s40623-024-02021-8.

Petrillo, G., Landes, F., Lippiello, E., and Rosso, A. The influence of the brittle-ductile transition zone on aftershock and foreshock occurrence. *Nature Communications*, 11:1–10, 2020. doi: 10.1038/s41467-020-16811-7.

Petrillo, G., Kumazawa, T., Napolitano, F., Capuano, P., and Zhuang, J. Fluids-triggered swarm sequence supported by a nonstationary epidemic-like description of seismicity. *Seismological Research Letters*, 95(6):3207–3220, 2024a. doi: 10.1785/0220240056.

Petrillo, G., Lippiello, E., and Zhuang, J. Including stress relaxation in point-process model for seismic occurrence. *Geophysical Journal International*, 236(3):1332–1341, 2024b. doi: 10.1093/gji/ggad482.

Pino, N. A., Convertito, V., Godano, C., and Piromallo, C. Subduction age and stress state control on seismicity in the NW Pacific subducting plate. *Sci. Rep*, 12(1):12440, 2022. doi: 10.1038/s41598-022-16076-8.

Pure, L. R., Leonard, G. S., Townsend, D. B., Wilson, C. J., Calvert, A. T., Cole, R. P., Conway, C. E., Gamble, J. A., and Bubs'Smith, T. A high resolution 40Ar/39Ar lava chronology and edifice construction history for Tongariro volcano, New Zealand. *Journal of Volcanology and Geothermal Research*, 403:106993, 2020. doi: 10.1016/j.jvolgeores.2020.106993.

Rodríguez-Pérez, Q., Monterrubio-Velasco, M., Zú niga, F. R., Valdés-González, C. M., and Arámbula-Mendoza, R. Spatial and temporal b-value characterization at Popocatépetl volcano, Central Mexico. *Journal of Volcanology and Geothermal Research*, 417:107320, 2021. doi: 10.1016/j.jvolgeores.2021.107320.

Sanchez, J. J., McNutt, S. R., Power, J., and Wyss, M. Spatial variations in the frequency-magnitude distribution of earthquakes at Mount Pinatubo Volcano. *Bulletin of the Seismological Society of America*, 94(2):430–438, 2004. doi: 10.1785/0120020244.

Scholz, C. The frequency-magnitude relation of microfracturing in rock and its relation to earthquakes. *Bull. seism. Soc. Am*, 58: 399–415, 1968. doi: 10.1785/bssa0580010399.

Shane, P. and Smith, V. C. Using amphibole crystals to reconstruct magma storage temperatures and pressures for the post-caldera collapse volcanism at Okataina volcano. *Lithos*, 156: 159–170, 2013. doi: 10.1016/j.lithos.2012.11.008.

Shi, Y. and Bolt, B. A. The standard error of the magnitude-

frequency b value. *Bulletin of the Seismological Society of America*, 72(5):1677–1687, 1982. doi: 10.1785/bssa0720051677.

Silva, R., Ferreira, T., Medeiros, A., Carmo, R., Luis, R., Wallenstein, N., Bean, C., and Sousa, R. Chapter 17 Seismic activity on S ao Miguel Island volcano-tectonic structures (Azores archipelago). *Geological Society, London, Memoirs*, 44(1):227–238, 2015. doi: 10.1144/m44.17.

Taroni, M., Zhuang, J., and Marzocchi, W. High-Definition Mapping of the Gutenberg–Richter b-Value and Its Relevance: A Case Study in Italy. *Seismological Research Letters*, XX:1–7, 2021. doi: 10.1785/0220210017.

Taroni, M., Petrillo, G., and Lippiello, E. Earthquake Size Distributions of Strong Worldwide Seismicity Are Similar for Background and Triggered Events. *Seismological Research Letters*, 2025. doi: 10.1785/0220240481.

Toda, S., Stein, R. S., and Sagiya, T. Evidence from the AD 2000 Izu islands earthquake swarm that stressing rate governs seismicity. *Nature*, 419(6902):58–61, 2002. doi: 10.1038/nature00997.

Tormann, T., Wiemer, S., and Mignan, A. Systematic survey of high-resolution b value imaging along Californian faults: Inference on asperities. *Journal of Geophysical Research: Solid Earth*, 119 (3):2029–2054, 2014. doi: 10.1002/2013JB010867.

Tramelli, A., Godano, C., Ricciolino, P., Giudicepietro, F., Caliro, S., Orazi, M., De Martino, P., and Chiodini, G. Statistics of seismicity to investigate the Campi Flegrei caldera unrest. *Scientific reports*, 11(1):7211, 2021. doi: 10.1038/s41598-021-86506-6.

Triantafyllou, I., Papadopoulos, G. A., Siettos, C., and Spiliotis, K. Real-time foreshock–aftershock–swarm discrimination during the 2025 seismic crisis near Santorini Volcano, Greece: earthquake statistics and complex networks. *Geosciences*, 15(8):300, 2025. doi: 10.3390/geosciences15080300.

Utsu, T., Ogata, Y., S, R., and Matsu'ura. The Centenary of the Omori Formula for a Decay Law of Aftershock Activity. *Journal of Physics of the Earth*, 43(1):1–33, 1995. doi: 10.4294/jpe1952.43.1.

van der Elst, N. J. B-positive: A robust estimator of aftershock magnitude distribution in transiently incomplete catalogs. *Journal of Geophysical Research: Solid Earth*, 126(2):e2020JB021027, 2021a. doi: 10.1029/2020jb021027.

van der Elst, N. J. B-positive: A robust estimator of aftershock magnitude distribution in transiently incomplete catalogs. *Journal of Geophysical Research: Solid Earth*, 126(2):e2020JB021027, 2021b. doi: 10.1029/2020jb021027.

Wang, Q., Jackson, D. D., and Zhuang, J. Are spontaneous earthquakes stationary in California? *Journal of Geophysical Research: Solid Earth*, 115(B8), 2010. doi: 10.1029/2009jb007031.

Westerhaus, M., Wyss, M., Yilmaz, R., and Zschau, J. Correlating variations of b values and crustal deformations during the 1990s may have pinpointed the rupture initiation of the Mw = 7.4 Izmit earthquake of 1999 August 17. *Geophysical Journal International*, 148(1):139–152, 2002. doi: 10.1046/j.0956-540x.2001.01554.x.

Wiemer, S. and McNutt, S. R. Variations in the frequency-magnitude distribution with depth in two volcanic areas: Mount St. Helens, Washington, and Mt. Spurr, Alaska. *Geophysical research letters*, 24(2):189–192, 1997. doi: 10.1029/96gl03779.

Wiemer, S. and Wyss, M. Mapping the frequency-magnitude distribution in asperities:An improved technique to calculate recurrence times? *J. Geophys. Res*, 102:15,115–15,128, 1997. doi: 10.1029/97jb00726.

Wiemer, S. and Wyss, M. Mapping spatial variability of the frequency-magnitude distribution of earthquakes. *Adv. Geophys*, 45:259–302, 2002. doi: 10.1016/s0065-2687(02)80007-3.

Wiemer, S., McNutt, S. R., and Wyss, M. Temporal and three-dimensional spatial analyses of the frequency–magnitude distribution near Long Valley Caldera, California. *Geophysical Journal International*, 134(2):409–421, 1998. doi: 10.1046/j.1365-246x.1998.00561.x.

Wyss, M. Towards a Physical Understanding of the Earthquake Frequency Distribution. *Geophysical Journal of the Royal Astronomical Society*, 31(4):341–359, 1973. doi: 10.1111/j.1365-246X.1973.tb06506.x.

Xiong, Z. and Zhuang, J. SETAS: A spherical version of the space–time ETAS model. *Seismological Society of America*, 94(3): 1676–1688, 2023. doi: 10.1785/0220220198.

Zaccagnino, D., Michas, G., Telesca, L., and Vallianatos, F. Precursory patterns, evolution and physical interpretation of the 2025 Santorini-Amorgos seismic sequence. *Earth and Planetary Science Letters*, 671:119656, 2025. doi: 10.1016/j.epsl.2025.119656.